Topological aspects of fermions on a honeycomb lattice

JHEP06(2009)060

(http://iopscience.iop.org/1126-6708/2009/06/060)

Published by IOP Publishing for SISSA

Received: *April 14, 2009*
Revised: *May 29, 2009*
Accepted: *June 6, 2009*
Published: *June 19, 2009*

Topological aspects of fermions on a honeycomb lattice

Dipankar Chakrabarti,[1] **Simon Hands and Antonio Rago**

Department of Physics, Swansea University,
Singleton Park, Swansea, SA2 8PP, U.K.

E-mail: dipankar@iitk.ac.in, s.hands@swan.ac.uk, a.rago@swan.ac.uk

Abstract: We formulate a model of relativistic fermions moving in two Euclidean dimensions based on a tight-binding model of graphene. The eigenvalue spectrum of the resulting Dirac operator is solved numerically in smooth U(1) gauge field backgrounds carrying an integer-valued topological charge Q, and it is demonstrated that the resulting number of zero-eigenvalue modes is in accord with the Atiyah-Singer index theorem applied to two continuum flavors. A bilinear but gauge non-invariant chirality operator appropriate for distinguishing the topological zero modes is identified. When this operator is used to calculate Q, it is found that the maximum topological charge capable of being measured in this fashion scales with the perimeter of the lattice. Some concluding remarks compare these results to what is known for staggered lattice fermions.

Keywords: Lattice Gauge Field Theories, Nonperturbative Effects, Lattice Quantum Field Theory

ArXiv ePrint: 0904.1310

[1]Present address: Department of Physics, Indian Institute of Technology Kanpur, Kanpur-208016, India.

doi:10.1088/1126-6708/2009/06/060

JHEP06(2009)060

Contents

1 Introduction

Following pioneering work in the 1980's [1], there has been a recent revival of interest in lattice fermion formulations with a minimal flavor content of chirally-symmetric fermions [2–5]. Stimulated by the excitations known to obey a quasi-relativistic Dirac equation in graphene (a monolayer of carbon atoms arranged in a honeycomb lattice which has recently been realised experimentally), Creutz [2] devised a four-dimensional Euclidean lattice action describing two species of massless chirally-invariant fermion, each centred at a special location $\pm\tilde{p}_\mu$ in momentum space. Creutz's action is formulated on a hypercubic lattice, with tunable parameters enabling the magnitude of $\tilde{p}_\mu$ to be controlled. Boriçi [3] soon developed the idea, finding an action with two flavors located this time at the origin and at $(\frac{\pi}{2a}, \frac{\pi}{2a}, \frac{\pi}{2a}, \frac{\pi}{2a})$. In each case the flavor content is the minimum consistent with the celebrated no-go theorem governing lattice fermion actions which are local, unitary, and chirally symmetric [6]. This has led to hopes that these formulations could form the basis for an inexpensive alternative to overlap fermions in realistic lattice QCD simulations with two light quark flavors.

The feature of these actions is that in the vicinity of the special "Dirac points" the eigenvalues E of a suitably-defined Hamiltonian operator can be written as $E(p_\mu - \tilde{p}_\mu) = \pm K|z(p)|$, where $z(p)$ can be written as $z_0 e^{i\theta}$ in two Euclidean dimensions and as $z_0 + i\vec{z}.\vec{\sigma}$ in four dimensions [2]. In $2d$ z maps an S^1 surrounding the Dirac point to a complex phase: in $4d$ the analogous mapping is from S^3 to a quaternionic space. In either case the solution of the fermion Hamiltonian engenders a non-trivial wrapping, implying that the

JHEP06(2009)060

surface must enclose a zero, so that the only consistent result on shrinking it to a point is $E = 0$. Hence the existence of the Dirac points, and the linear nature of the dispersion $E(p_\mu - \tilde{p}_\mu)$ in their immediate vicinity, is topologically stable.[1] One might therefore hope that the desirable properties listed above persist even once interactions with gauge degrees of freedom are introduced.

A difficulty has been pointed out in [4]; the actions of [2, 3], while chirally symmetric, break important hypercubic and discrete symmetries such as parity and time-reversal, meaning that they are not protected against acquiring non-covariant counterterms such as eg. $\bar{\psi}\gamma_\mu\psi$ through quantum corrections. This introduces a severe fine-tuning problem to any practical simulation programme based on the original actions. Recently Creutz has proposed a refinement of the action of [3] in which it is claimed such effects can be mitigated to the point where perhaps they are manageable [7].

The purpose of the current paper is to investigate the interaction of these minimal chiral fermions with gauge fields, not via a perturbative approach to radiative corrections [4, 5], but rather in a non-perturbative manner via their response to a globally-defined topological charge. It is well-known that in a gauge background with integer-valued topological charge Q, the spectrum of the Dirac operator D obeys the Atiyah-Singer index theorem

$$Q = n_+ - n_-, \tag{1.1}$$

where $n_{+(-)}$ denotes the number of positive (negative) chirality zero modes of D. We have been inspired by the classic paper [8] of Smit and Vink, who studied the extent to which (1.1) is obeyed for both staggered and Wilson lattice fermions. Accordingly, we will investigate the response of minimal chiral fermions in $2d$ by calculating the spectrum of D in a background U(1) gauge field corresponding to a quantised homogeneous flux, which can be shown to carry $Q \neq 0$. Because of the combination of apparent simplicity with high symmetry, we have chosen to track closely the original connection with graphene and hence formulate our fermions on a honeycomb lattice. In $4d$ the analogous "hyperdiamond" lattice corresponds to a particular choice of parameters in [2], and has been explored further in [9]. Despite the aesthetic appeal of the honeycomb, it presents technical challenges which we feel are worth reporting in some detail. We will show that the index theorem (1.1) is indeed satisfied, and find a definition of chirality $\bar{\psi}\sigma_3\psi$ capable of distinguishing between zero and non-zero modes. The drawback is that it is not gauge-invariant, and may not even be universal.

The special properties of fermions hopping on a honeycomb lattice have been known in the literature for many years, ever since Semenoff [10] noted the relativistic nature of the dispersion around the Dirac points and solved the resulting Dirac equation in a homogeneous magnetic field in the long-wavelength limit to expose topologically-stable zero modes, confirming a result found in continuum field theory by Jackiw [11]. More recently, the topological aspects of honeycomb fermions interacting with an external magnetic field have been used to account for the unconventional quantum Hall effect in graphene [12]. The

[1] Because of the periodicity of the Brillouin Zone, the Dirac points must appear in pairs so that the overall wrapping vanishes [6].

JHEP06(2009)060

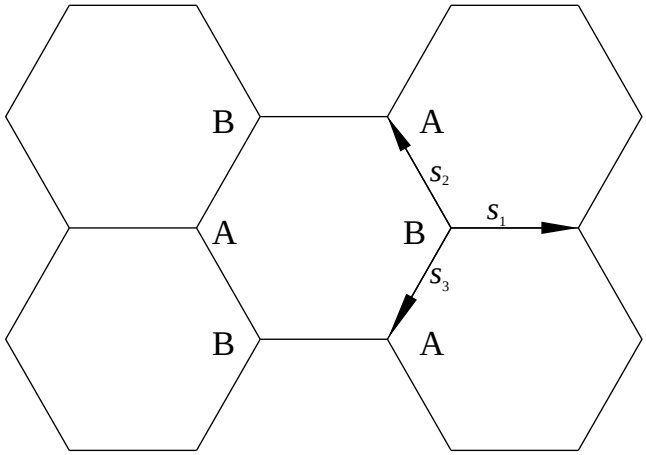

Figure 1. Honeycomb lattice.

index theorem has also been used to analyse the effects of point defects in graphene [13]. In these papers the authors either worked in the continuum limit of the lattice model or worked in momentum space. In this work, by contrast, we will examine the applicability of the continuum results to fermions defined on the finite lattices relevant for QCD simulations; our concerns will be the approach to and recovery of the continuum limit predictions, and the technical issues associated with defining a chirality operator referrred to in the previous paragraph.

The remainder of the paper is organised as follows. In section 2 we specify the honeycomb lattice, define the lattice Dirac operator, and show that in the long-wavelength limit an action describing two continuum Dirac flavors is recovered. Section 3 reviews the index theorem, and outlines how U(1) configurations with $Q \neq 0$ may be constructed on the honeycomb, and section 4 presents the Dirac spectrum calculated both for free fermions on the honeycomb, and for continuum fermions on backgrounds with $Q \neq 0$. In section 5 we then present numerical results for the spectrum calculated on lattices up to size 100×100 with $Q \neq 0$. The definition used for the chirality of a mode differs from the naive expectation based on free fermions. Nonetheless, we will show that both the spectrum and the index calculated on the basis of this chirality match analytic expectations provided Q is not too large; interestingly, the maximum value of Q for which continuum results are reproduced turns out to scale with the perimeter of the lattice. Our concluding remarks in section 6 will contrast what we have found with what is known for staggered lattice fermions. Some technical details concerning the definition of the Fourier transform on a finite honeycomb lattice are postponed to an appendix.

2 Lattice action

It is convenient to begin our presentation using a Hamiltonian devised for physical (ie. $2+1$-dimensional) graphene [14]. It is assumed that on each site $\mathbf{r}$ of a honeycomb lattice there is a mobile electron which may hop to a neighbouring site under the constraints of

JHEP06(2009)060

the Pauli Exclusion Principle. Electron spin may be ignored for now; the tight-binding Hamiltonian is then

$$H = -t \sum_{\mathbf{r}\in B} \sum_{i=1}^{3} b^\dagger(\mathbf{r}) U(\mathbf{r}, \mathbf{s}_i) a(\mathbf{r}+\mathbf{s}_i) + a^\dagger(\mathbf{r}+\mathbf{s}_i) U^\dagger(\mathbf{r}, \mathbf{s}_i) b(\mathbf{r}), \tag{2.1}$$

where t is a hopping parameter, $\mathbf{s}_i (i = 1, 2, 3)$ are the three vectors along the links as shown in figure 2:

$$\mathbf{s}_1 = (1, 0)l, \quad \mathbf{s}_2 = \left(-\frac{1}{2}, \frac{\sqrt{3}}{2}\right)l, \quad \mathbf{s}_3 = \left(-\frac{1}{2}, -\frac{\sqrt{3}}{2}\right)l, \tag{2.2}$$

and l is the honeycomb bond length. The sites labelled A and B belong to inequivalent sublattices, on which the operators $a^\dagger$ (a) and $b^\dagger$ (b) respectively create (destroy) fermions. The variable $U(\mathbf{r}, \mathbf{s}_i)$ is a U(1)-valued gauge connection emerging from the B site at $\mathbf{r}$ along $\mathbf{s}_i$. The Hamiltonian (2.1) is thus invariant under U(1) gauge transformations.

To expose the relativistic nature of the low-energy excitation spectrum, define $H_0 = H[U = 1]$ and transform to momentum space (we will refine our definition of the Fourier transformation during the course of what follows):

$$H_0 = \sum_{\vec{k}} \left(\Phi(\vec{k}) a^\dagger(\vec{k}) b(\vec{k}) + \Phi^*(\vec{k}) b^\dagger(\vec{k}) a(\vec{k}) \right) \tag{2.3}$$

with

$$\Phi(\vec{k}) = -t \left[e^{ik_x l} + 2\cos\left(\frac{\sqrt{3}k_y l}{2}\right) e^{-i\frac{k_x l}{2}} \right]. \tag{2.4}$$

Consider a basis of Fock states $|\vec{k}_\pm\rangle = (\sqrt{2})^{-1}[a^\dagger(\vec{k}) \pm b^\dagger(\vec{k})]|0\rangle$ where $a|0\rangle = b|0\rangle = 0$, $\{a^\dagger(\vec{k}), a(\vec{k}')\} = \delta^2(\vec{k} - \vec{k}')$, $\{a, a\} = \{a^\dagger, a^\dagger\} = 0$ etc. It is straightforward to see that $\langle \vec{k}_\pm | H_0 | \vec{k}_\pm \rangle = \pm(\Phi(\vec{k}) + \Phi^*(\vec{k})) \equiv \pm E(\vec{k})$, and hence that the spectrum is symmetric about zero. At half-filling (one electron per site) the Fermi energy is thus at $E = 0$.

The dispersion relation $E(\vec{k})$ vanishes not at $\vec{k} = \vec{0}$, but at the six corners of the first Brillouin zone, which is also a hexagon but rotated by 90° with respect to the cells of figure 2. The corners of this hexagon lie at the centres of inequivalent equilateral triangles formed from reciprocal lattice points; the Brillouin zone thus contains two inequivalent *Dirac points* around which an effective low-energy description can be built, which we will take as $\vec{K}_\pm = (0, \pm\frac{4\pi}{3\sqrt{3}l})$. Around these points we can expand:

$$\Phi(\vec{K}_\pm + \vec{p}) = \pm v_F [p_y \mp i p_x] + O(p^2) \tag{2.5}$$

where the Fermi velocity $v_F = \frac{3}{2}tl$. It is now possible, by defining field operators in the neighbourhood of the Dirac points via $a_\pm(\vec{p}) = a(\vec{K}_\pm + \vec{p})$ etc, to recast the Hamiltonian in relativistic form:

$$H_0 \simeq v_F \sum_{\vec{p}} \Psi^\dagger(\vec{p}) \vec{\alpha}.\vec{p} \Psi(\vec{p}) \tag{2.6}$$

where Ψ is the column vector $(b_+, a_+, a_-, b_-)^T$ and the 4×4 matices $\vec{\alpha}$ are defined by

$$\alpha_x = \begin{pmatrix} -\sigma_2 & \\ & \sigma_2 \end{pmatrix}; \quad \alpha_y = \begin{pmatrix} \sigma_1 & \\ & -\sigma_1 \end{pmatrix} \tag{2.7}$$

so that $\{\alpha_i, \alpha_j\} = 2\delta_{ij}$. In this form H_0 is easily seen to be proportional to the Dirac Hamiltonian describing a single massless four-component spinor moving with speed v_F. For physical graphene, the Hamiltonian (2.1) must be modified to incorporate electron spin; this results in a relativistic $d = 2 + 1$ model with two four-component flavors.

Starting from the Hamiltonian (2.1) an action for chiral gauge theory in $d = 2+1$ was proposed by Jackiw and Pi in [14]. In this paper we instead recast it as a $d = 2$ Euclidean quantum field theory with action of the form $S = \bar{\chi} D \chi$, describing two species of fermion field sitting on a honeycomb lattice, each species occupying a distinct sublattice. The resulting equation of motion resembles the Dirac equation in the long wavelength limit; the Dirac operator D can be written as

$$\begin{aligned}(D\chi)(x) = {} & D_1(x+\hat{0})\chi(x+\hat{0}) + D_1(x-\hat{0})\chi(x-\hat{0}) + D_2(x+\hat{2})\chi(x+\hat{2}) \\ & + D_2(x-\hat{2})\chi(x-\hat{2}) + D_3(x)\chi(x). \end{aligned} \tag{2.8}$$

In writing the operator this way we have introduced the notion of a *lattice* of identical A sites, with rhombus-shaped unit cells of side $a = \sqrt{3}l$ each containing one A site and one B site (see figure 2). Each cell is indexed by a vector x, whose form will be specified below, and primitive vectors $\hat{0} = \mathbf{s}_1 - \mathbf{s}_3$ and $\hat{1} = \mathbf{s}_2 - \mathbf{s}_1$ define the lattice axes. It is also convenient to define the dependent vector $\hat{2} = \hat{0} + \hat{1}$. The different elements of the operator are then written

$$\begin{aligned} D_1(x+\hat{0}) &= \begin{pmatrix} 0 & 0 \\ U(x, \mathbf{s}_1) & 0 \end{pmatrix}, & D_1(x-\hat{0}) &= \begin{pmatrix} 0 & U^*(x-\hat{0}, \mathbf{s}_1) \\ 0 & 0 \end{pmatrix}, \\ D_2(x+\hat{2}) &= \begin{pmatrix} 0 & 0 \\ U(x, \mathbf{s}_2) & 0 \end{pmatrix}, & D_2(x-\hat{2}) &= \begin{pmatrix} 0 & U^*(x-\hat{2}, \mathbf{s}_2) \\ 0 & 0 \end{pmatrix}, \\ D_3(x) &= \begin{pmatrix} 0 & U^*(x, \mathbf{s}_3) \\ U(x, \mathbf{s}_3) & 0 \end{pmatrix}, \end{aligned} \tag{2.9}$$

with the spinors

$$\chi(x) = \begin{pmatrix} \chi_A(x) \\ \chi_B(x) \end{pmatrix} \tag{2.10}$$

where $\chi_A(x)$ and $\chi_B(x)$ are single-component Grassmann fields located at sites A and B of cell x respectively.

Note that with our definition of the link directions all terms in the action are either of the form $\bar{\chi}_B U \chi_A$ or $\bar{\chi}_A U^* \chi_B$. While the antihermiticity of the Dirac operator (2.8), (2.9) is not manifest, a little care and close inspection of figures 2, 3 will convince the reader that this is indeed the case. The above analysis expanding S about the Dirac points $\vec{k} = \vec{K}_\pm$ goes

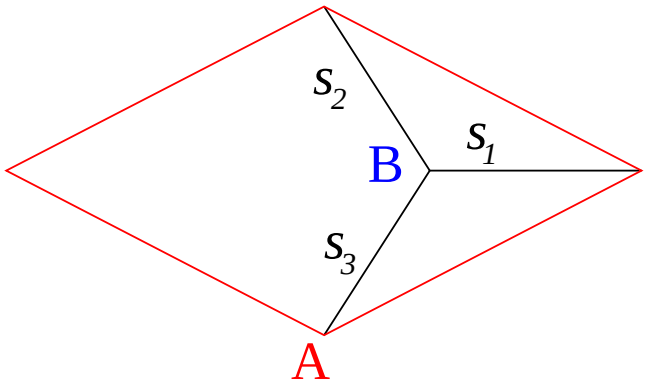

Figure 2. The primitive cell.

through as before; writing $\psi_1 = (\chi_{B+}, \chi_{A+})^T$, $\bar{\psi}_1 = (\bar{\chi}_{B+}, \bar{\chi}_{A+})$, $\psi_2 = (-\chi_{A-}, -\chi_{B-})^T$ and $\bar{\psi}_2 = (\bar{\chi}_{A-}, \bar{\chi}_{B-})$, with $\chi_{A\pm}(\vec{p}) = \chi_A(\vec{K}_\pm + \vec{p})$ as before, we obtain

$$S_0 \simeq \frac{3l}{2} \sum_{\vec{p}} \sum_{\alpha=1}^{2} \bar{\psi}_\alpha \vec{p}.\vec{\sigma} \psi_\alpha, \tag{2.11}$$

that is, a relativistically covariant action describing two flavors of two-component spinor moving in $d = 2$ Euclidean dimensions, each flavor localised at one single Dirac point. Chirality is then *naively* defined by the bilinear

$$\bar{\psi}_\alpha \sigma_3 \psi_\alpha = \bar{\chi}_{B+}\chi_{B+} - \bar{\chi}_{A+}\chi_{A+} - \bar{\chi}_{A-}\chi_{A-} + \bar{\chi}_{B-}\chi_{B-} = \bar{\chi}_B \chi_B - \bar{\chi}_A \chi_A, \tag{2.12}$$

where the second equality assumes that all parts of momentum space can be treated uniformly, leading in effect to a staggered order parameter. As we shall see in section 5 below, the definition needs to be modified in the presence of gauge fields.

To define a finite, translationally-invariant lattice we need to close the manifold by specifying boundary conditions. In this paper we have studied two distinct possibilities. The technically simpler choice is to close the manifold along the two non-orthogonal axes $\hat{0}$ and $\hat{1}$, for instance defining an $L_0 \times L_1$ system by requiring $f(x + L_0\hat{0}) = f(x + L_1\hat{1}) = f(x)$. We call this the "primitive" lattice shown in red in figure 4. Note it contains $L_0 L_1$ distinct hexagons. We can alternatively choose to implement the boundary conditions along the orthogonal axes $\hat{X}$ and $\hat{Y}$, in this case calling it the "perpendicular" lattice shown in black in figure 3. Some care is needed in indexing the lattice this way: it is convenient to assign the two A sites $\mathbf{r}$ and $\mathbf{r} - \mathbf{s}_3 + \mathbf{s}_2$ and the B site $\mathbf{r} - \mathbf{s}_3$ the same $\hat{X}$ index, but to assign them $\hat{Y}$ indices of respectively eg. 0, $\frac{1}{2}$, and 1. In this way a lattice which extends L_X units along $\hat{X}$ and L_Y units along $\hat{Y}$ contains $L_X L_Y$ distinct hexagons.

3 Index theorem

Let us consider fermions in the presence of a topological charge Q created by a background gauge field configuration. In the continuum, the Atiyah-Singer index theorem relates the

JHEP06(2009)060

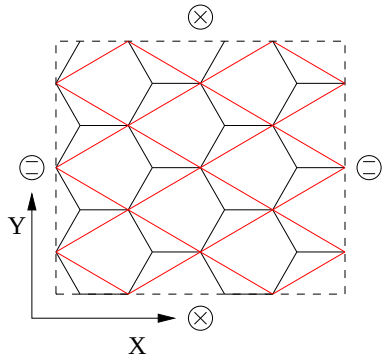

Figure 3. Perpendicular compactification.

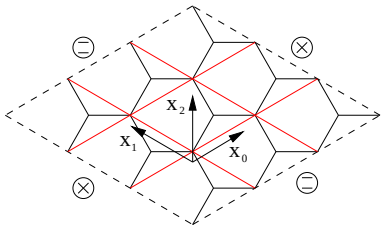

Figure 4. Primitive compactification.

topological charge to the number of chiral zero modes of the fermion. If ψ_i are the eigenstates of the antihermitian Dirac operator with eigenvalue iE_i, then

$$Q = \sum_{i,E_i=0} \psi_i^\dagger \gamma_5 \psi_i = n_+ - n_-, \tag{3.1}$$

where $n_{+(-)}$ is the number of zero eigenvalue modes of positive (negative) chirality, ie. satisfying $\gamma_5 \psi_i = \pm \psi_i$. A heuristic derivation of this relation for lattice fermions is given in [8]. Since chiral symmetry is minimally broken, we anticipate the above relation holds good on a honeycomb lattice with a suitable generalisation of the chirality operator γ_5.

In two Euclidean dimensions topological charge density is proportional to the magnetic field strength tensor F_{12}. The two-dimensional analogues of instantons are localised vortices carrying a quantised magnetic flux; the topological charge Q is defined by

$$Q = \frac{1}{2\pi} \int d^2x F_{12}. \tag{3.2}$$

On a finite system it is also possible to define homogeneous backgrounds with $Q \neq 0$. Consider the abelian field strength tensor $F_{12} = \partial_x A_y - \partial_y A_x$ on a $2d$ system with boundaries closed in orthogonal directions. Following [8], we then choose $A_x(x, y) = -\omega y$ and $A_y(x, y) = 0$, so that $F_{12} = \omega$. On a $L_x \times L_y$ square lattice of spacing a the gauge field A_1 at the boundary $y = L_y a$ is related to that at $y = 0$ by a gauge transformation [8]

$$A_x(y = 0) = A_x(y = L_y a) + i\Omega_y \partial_x \Omega_y^{-1} \tag{3.3}$$

where

$$\Omega_y(x, y) = e^{i\omega L_y a x}. \tag{3.4}$$

JHEP06(2009)060

The discontinuity is permitted since any gauge invariant object remains continuous across the boundary of the lattice. Demanding periodicity in the x-direction as well results in a field strength quantised consistently with (3.2):

$$\omega = \frac{2\pi}{L_x L_y a^2} Q. \tag{3.5}$$

On the honeycomb lattice the gauge background with constant field strength ω over the lattice, and accordingly equal flux $\omega\mathcal{A}$ through each hexagonal plaquette of area $\mathcal{A} = \frac{\sqrt{3}}{2}a^2$, is quantised according to

$$\omega = \frac{4\pi}{\sqrt{3} L_x L_y a^2} Q. \tag{3.6}$$

The link field configuration depends on which boundary condition we consider. For the primitive lattice boundary condition, a possible choice is:

$$U(x, \mathbf{s}_1) = \exp\left(-i\frac{\sqrt{3}}{2}\omega x_0 a^2\right); \quad U(x, \mathbf{s}_2) = 1; \quad U(x, \mathbf{s}_3) = 1, \tag{3.7}$$

for all cells except those of the last row with $x_0 = L_0 - 1$ where in addition we require

$$U(x_0 = L_0 - 1, x_1, \mathbf{s}_3) = \exp\left(-i\frac{\sqrt{3}}{2}\omega L_0 x_1 a^2\right). \tag{3.8}$$

It is readily checked that each hexagonal plaquette then has the value $\exp(i\omega\mathcal{A})$.

For the perpendicular boundary condition, a link field configuration for the same constant field strength ω could be chosen as follows. For $x_Y = 0, \frac{1}{2}, 1, \ldots, L_Y - \frac{1}{2}$:

$$U(x, \mathbf{s}_1) = \exp\left(-i\frac{\sqrt{3}}{2}\omega x_Y a^2\right); \quad U(x, \mathbf{s}_2) = 1; \quad U(x, \mathbf{s}_3) = 1, \tag{3.9}$$

whereas for the links in the last row we need

$$\begin{aligned} U(x_Y = L_Y - \tfrac{1}{2}, x_X, \mathbf{s}_2) &= \exp\left(i\frac{\sqrt{3}}{4}\omega L_Y x_X a^2\right); \\ U(x_Y = L_Y, x_X, \mathbf{s}_3) &= \exp\left(i\frac{\sqrt{3}}{4}\omega L_y x_X a^2\right). \end{aligned} \tag{3.10}$$

4 Dirac spectrum: analytic results

With the above gauge field configuration we need to solve the lattice Dirac equation

$$D\chi_i = iE_i\chi_i \tag{4.1}$$

with $\chi_i(x)$ satisfying primitive or perpendicular boundary conditions as appropriate. For an arbitrary gauge field background we can do only that numerically. In this section we first discuss the spectrum on a honeycomb lattice without any gauge field, and then for a continuum Dirac operator on a smooth background field with $Q \neq 0$ of the kind outlined in section 3.

If we consider the boundary condition on the primitive lattice and in the free field limit, a plane wave ansatz gives the eigenvalues

$$E(k_0, k_1) = \pm\sqrt{3 + 2\cos k_0 + 2\cos(k_0 - k_1) + 2\cos k_1}. \tag{4.2}$$

For periodic boundary conditions along $\hat{0}$ and $\hat{1}$, the allowed momentum modes are given by

$$\begin{aligned} k_0 &= \frac{2\pi n_0}{L_0}, \quad n_0 = 0, 1, 2, \cdots L_0 - 1; \\ k_1 &= \frac{2\pi n_1}{L_1}, \quad n_1 = 0, 1, 2, \cdots L_1 - 1. \end{aligned} \tag{4.3}$$

Note that $k_0\hat{0}$ and $k_1\hat{1}$ are not orthogonal. One can clearly see that $E(k_0, k_1)$ is not minimised at $k_0 = k_1 = 0$, but rather at the Dirac points $K_\pm = (\mp\frac{2\pi}{3}, \pm\frac{2\pi}{3})$: recovering the continuum relativistic dispersion relation is therefore nontrivial. Writing $k = K_\pm + q$, the leading term in the expansion is

$$E(q_0, q_1) = \pm\sqrt{q_0^2 - q_0 q_1 + q_1^2}. \tag{4.4}$$

Replacing the non-orthogonal $q_0,\ q_1$ by orthogonal momenta $p_x,\ p_y$ via $q_{0,1} = p_x \pm \frac{1}{\sqrt{3}} p_y$, we get the desired relativistic dispersion relation

$$E(p_x, p_y) = \pm\sqrt{{p_x}^2 + {p_y}^2}. \tag{4.5}$$

If expressions (4.2- 4.5) are required in terms of dimensionful momenta $\tilde{k}, \tilde{q}, \tilde{p}$, then note that $p = a\tilde{p}$ etc.

The solution for a single flavor of Dirac fermion moving in a $2d$ uniform background magnetic flux density ω was first discussed in [11]; here we review the explict solution given in [8]. The equation is written

$$D\psi_j = \sum_{\mu=1}^{2} D_\mu \sigma_\mu \psi_j = iE_j\psi_j, \tag{4.6}$$

where ψ is a two-component spinor. For a background with topological charge $Q \neq 0$ there are $|Q|$ independent solutions of the form (with $a = 1$):

$$\psi_{n\pm}(x, y) \propto \sum_{\ell=-\infty}^{\infty} e^{2\pi i \frac{x}{L_x}(j+\ell|Q|)} e^{-\frac{1}{2}|\omega|(y \pm \frac{L_y}{|Q|}(j+\ell|Q|))^2} H_n\left(\sqrt{|\omega|}(y \pm \frac{L_y}{|Q|}(j + \ell|Q|))\right) \phi_\pm, \tag{4.7}$$

where $j = 0, 1, \ldots, |Q| - 1$, $\phi_+ = \begin{pmatrix} 0 \\ 1 \end{pmatrix}$, $\phi_- = \begin{pmatrix} 1 \\ 0 \end{pmatrix}$, H_n are Hermite polynomials of order n, and Q and ω are related via (3.2). The corresponding eigenvalues are given by

$$E_{n\pm}^2 = (2n + 1)|\omega| \mp \omega. \tag{4.8}$$

Rearranging, we find a spectrum

$$E_m^2 = 2m|\omega|, \quad m = 0, 1, 2, \ldots \tag{4.9}$$

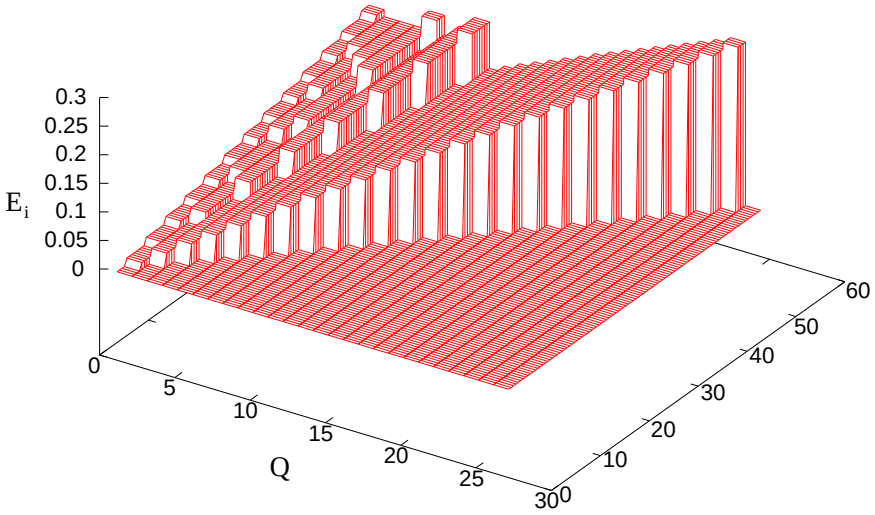

Figure 5. Eigenvalue spectrum as a function of Q on a 30×30 lattice (the vertical scale is measured in units where $a^{-2} = \frac{\sqrt{3}}{2}$).

with degeneracy

$$g_m = \begin{cases} |Q| & m = 0; \\ 2|Q| & m > 0. \end{cases} \tag{4.10}$$

The $|Q|$ zero modes are all proportional to ϕ_+ (ϕ_-) for Q positive (negative), in accordance with the index theorem (3.1). For $m > 0$ an equal number of positive and negative chirality solutions can be found. The increase of g_m with ω is a relativistic analogue of the Landau levels observed in metals in a strong magnetic field. For the two continuum flavors described by the honeycomb Dirac operator (2.8), the index theorem thus predicts $2|Q|$ zero modes, a result first obtained in [10].

5 Numerical results

In order to analyze the spectrum of the Dirac operator in various gauge field backgrounds, the matrix $-D^2[U]$ was diagonalised via a subspace iteration technique, using Chebyshev polynomial iteration to accelerate the convergence of the eigenvalues E^2. Since small eigenvalues converge at a faster rate than the high lying eigenvalues, locking the already converged eigenvalues and eigenvectors also accelerates the convergence of the other eigenvalues. The locked eigenspaces are only used to orthogonalise the remaining subspaces. This algorithm is also suitable to find the few lowest lying eigenvectors. Further details may be found in [15, 16].

In figure 5 we plot the 60 smallest eigenvalues E^2 calculated on a 30×30 lattice with primitive boundary conditions, for values of topological charge Q varying between 1 and 26. The spectrum for the perpendicular boundary conditions is identical. On this lattice $\omega a^2 = 0.00698Q$. Close inspection of the figure reveals very good agreement with both the eigenvalue prediction (4.9) and the degeneracy pattern (4.10), recalling that for two flavors we expect a degeneracy $2g_m$. In particular, the triangular "carpet" with $E^2 = 0$ corresponds

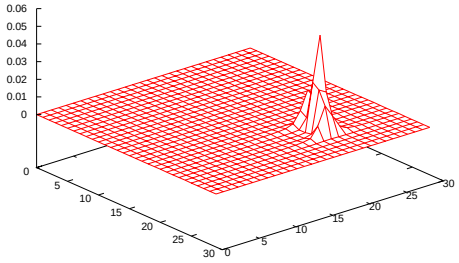

(a) $E = 0$, Multi-valued FT, A sublattice

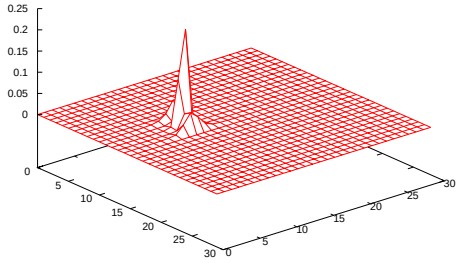

(b) $E = 0$, Multi-valued FT, B sublattice

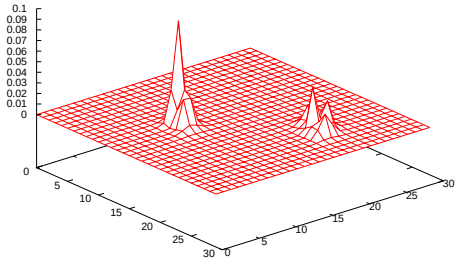

(c) $E \neq 0$, Multi-valued FT, A sublattice

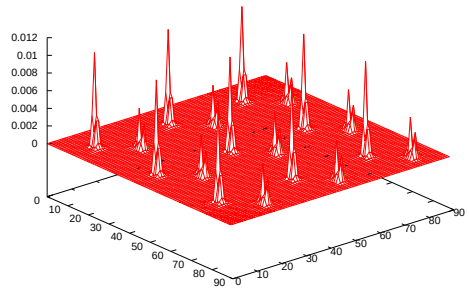

(d) $E \neq 0$, Single valued FT, A sublattice

Figure 6. Eigenvector profiles $|\chi|^2$ plotted in momentum space. Results taken on a 30×30 lattice with primitive boundary conditions.

to the zero modes with degeneracy growing linearly with Q as predicted by the index theorem (3.1). It is important to note that for these smooth background configurations the zero-mode eigenvalue is equal to zero within machine precision, just as is the case for staggered fermions [8]. In what follows we will strengthen this correspondence by specifying a chirality operator appropriate for honeycomb fermions.

In order to proceed, recall the discussion of section 2, and in particular that the low energy modes are located in the neighbourhood of the Dirac points, ie. away from the origin of momentum space. It is therefore helpful to perform analysis in momentum space by Fourier transforming the eigenvectors $\chi_i(x)$. It turns out that calculating the discrete Fourier transform on a honeycomb lattice is rather tricky [17], essentially because the range of k-values required for a unique invertible Fourier transform to exist is larger than is the case for a square lattice. As shown in the appendix, we have the choice of defining a single-valued transform ranging over either $6L_XL_Y$ (perpendicular) or $9L_0L_1$ (primitive) modes, or a multi-valued transform ranging over $2L_XL_Y$ (perpendicular) or L_0L_1 (primitive). This is exemplified in figure 6, where the single-valued transform shown in figure 6d to a very good approximation consists of nine copies of the multi-valued transform defined over a smaller range shown in figure 6c. In fact, while we have carried out all subsequent

JHEP06(2009)060

analysis using both variants of the Fourier transform, the results in all cases are found to be identical, as exemplified by figure 8 below.

In figure 6 we have chosen to transform the eigenvector densities on A and B sublattices separately to expose an important distinction between zero and non-zero modes. In each case the modes are tightly localised around two complementary locations in k-space, which we identify with the $\pm$ Dirac points discussed previously. However, while the non-zero mode of figures 6c,d clearly has support at both Dirac points, for the zero mode the eigenvector on the A sublattice is supported only near the + point (figure 6a) whereas on the B sublattice it is supported only near the - point (figure 6b).

This behaviour can be understood via the following heuristic argument. Consider solving the continuum problem on an infinite volume in a more symmetric gauge: $A_x = -\frac{\omega}{2}y$; $A_y = \frac{\omega}{2}x$. Solutions can readily be found of the form

$$\psi_{\ell\pm} \propto (x \mp iy)^\ell \exp\left(-\frac{|\omega|}{4}(x^2+y^2)\right)\phi_\pm \tag{5.1}$$

with corresponding eigenvalues

$$E^2_{\ell\pm} = (\ell+1)[|\omega| \mp \omega], \quad \ell = 0, 1, 2, \ldots \tag{5.2}$$

The spectrum (4.9), (4.10) is reproduced, with both chiralities contributing to non-zero modes, but with only positive chirality zero-modes present for $\omega > 0$ and *vice-versa*. However, in this gauge $\psi_{\ell\pm}$ is also an eigenstate of orbital angular momentum $\hat{L} = i(y\partial_x - x\partial_y)$ with eigenvalue $\mp\ell$. Physically, the $\psi_{\ell\pm}$ describe particles executing circular motion (the modes (5.1) are localised on annular regions centred at the origin) with opposite senses for + and − states - in other words the particle's charge and hence its response to a magnetic field is determined by its chirality. Now, in the rest frame both chiralities yield orbits of the same shape. However, for our honeycomb fermions the states are located at the Dirac points, and hence the previous picture needs to be Lorentz-boosted. A charged particle moving through a magnetic field with non-zero linear momentum has as trajectory a $2d$ projection of a helix; + and − particle states can no longer be superimposed and must therefore be described by different wavefunctions. Hence a state with a well-defined chirality is necessarily localised around a single point in k-space.

We learn from this argument that constructing states with well-defined continuum quantum numbers may not be straightforward for honeycomb fermions. In particular, the naive definition of chirality (2.12) derived for free fermions appears not to be suitable for the fermion modes in constant background flux of figure 6a,b , since in this case it receives cancelling contributions from A and B sublattices. Instead, we propose the following definition of chirality for interacting honeycomb fermions:

$$\bar{\psi}_\alpha \Sigma_3 \psi_\alpha = -\bar{\chi}_{B+}\chi_{B+} + \bar{\chi}_{A+}\chi_{A+} - \bar{\chi}_{A-}\chi_{A-} + \bar{\chi}_{B-}\chi_{B-}. \tag{5.3}$$

Equation (5.3) is evaluated in Fourier space, with each mode counted as + or − depending on which Dirac point it lies closer to.[2] We note in passing that the chirality operator

[2]The location of the Dirac point depends on the boundary conditions and in practice is determined by the maximum of $\bar{\chi}\chi$.

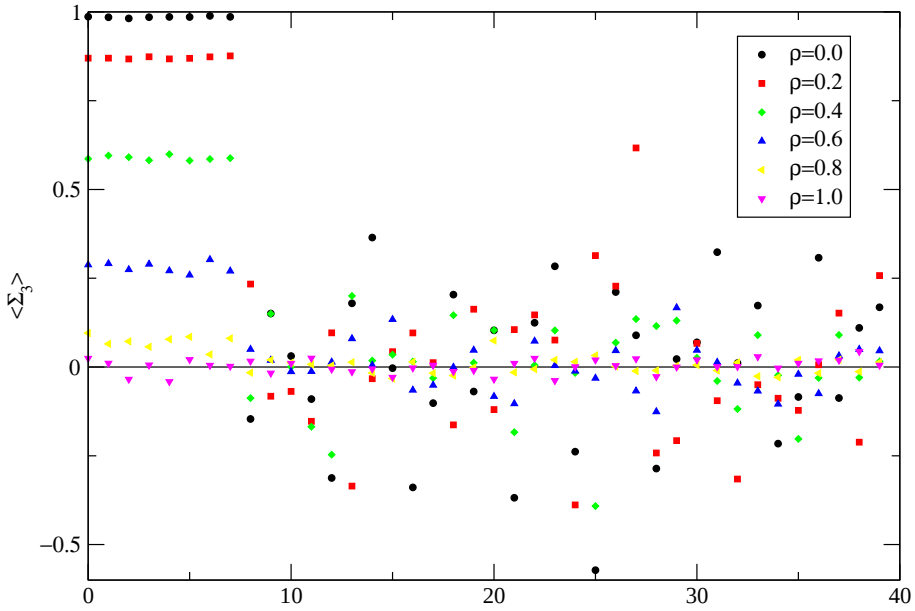

Figure 7. Chirality vs. mode number for various random gauge noise ρ.

introduced in the (2+1)-dimensional treatment of [14] also assigns opposite chiral charges to fields localised around the different Dirac points. In figure 7 we plot the expectation values of the chirality operator (5.3) evaluated on the lowest 40 eigenmodes of a 30×30 system with $Q = 4$. We have repeated the calculation, each time implementing a random gauge transformation of the form $e^{i\theta(\mathbf{r})\rho}$ at each site, where θ is uniformly distributed around the circle and ρ is a parameter. This transformation of course leaves the spectrum unchanged. For the smooth untransformed background the chirality $\langle\Sigma_3\rangle = +1$ to a good approximation for the $2|Q|$ topological zero modes. For non-zero modes the chirality has a smaller magnitude and a fluctuating sign; moreover its sum over all degenerate non-zero modes is exactly zero. Both of these are of course minimum requirements for a realistic chirality operator. However, figure 7 also confirms that the operator (5.3) is not gauge invariant, which is not surprising since it is formulated in momentum space. As the amplitude of the short-wavelength noise injected into the gauge background grows with ρ, the magnitude of $\langle\Sigma_3\rangle$ falls steadily, until eventually the zero and non-zero modes become indistinguishable. Using the definition (5.3) on backgrounds with $\rho = 0$ we present results for the topological charge Q^{index}, as evaluated via the index theorem (3.1) on the zero modes, versus the charge Q^{flux}, obtained by integrating the background flux (3.2), for a range of lattice sizes using both boundary conditions in figure 8. For Q not too large the curves fall on a straight line of unit slope independent of lattice volume, confirming the validity of the definition (5.3) and verifying the index theorem. However beyond some value of Q, which depends on L, the curves reach a maximum and then fall with increasing flux density. Different behaviour is observed for the two kinds of boundary condition but reassuringly, as mentioned above, the results are insensitive to which definition of the Fourier transform is used.

JHEP06(2009)060

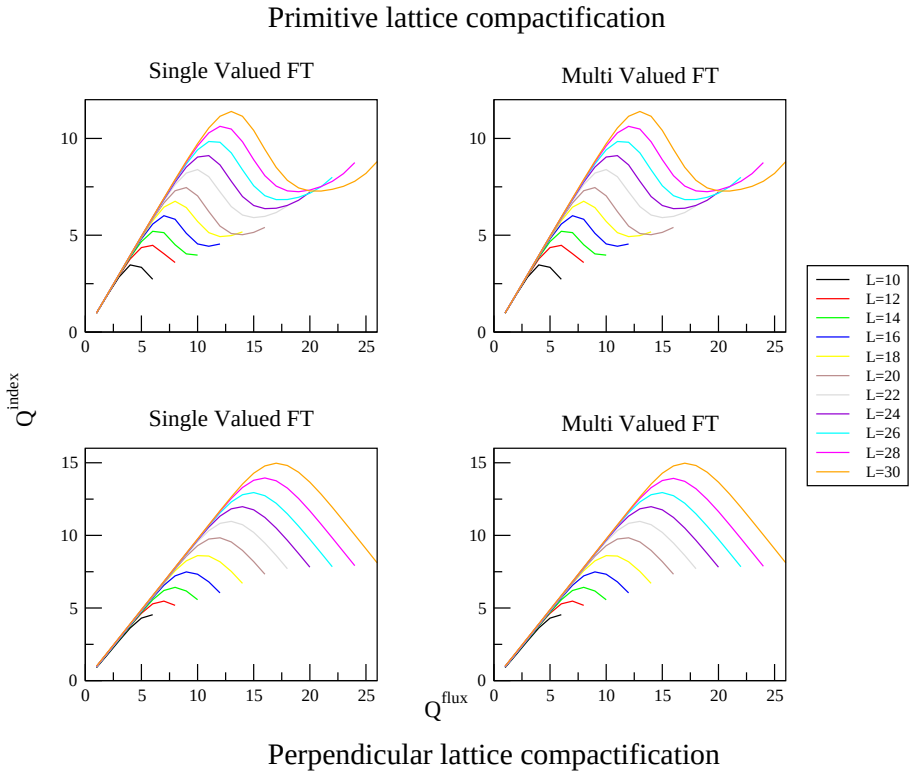

Figure 8. Q^{index} versus Q^{flux} for different lattices

In fact, the maximal topological charge achievable on a given lattice depends linearly on the length of its perimeter, rather than the area as naively one would expect. For instance in the case of an $L_X \times L_Y$ perpendicular compactification, provided that that a different scale factor for the X and Y directions is chosen, then the maximum achievable Q^{index} is linearly proportional to both L_X and L_Y independently. In particular in figure 9 we plot $Q^{\text{index}}_{\text{max}}$ as a function of "perimeter" $P = 3L_X + \frac{\sqrt{3}}{4}L_Y$ for all possible combinations of L_X and L_Y in the range 20-30 independently, plus for other larger lattices with $L_X = L_Y$. A possible interpretation of this phenomenon is that for a $2d$ U(1) gauge theory with constant magnetic flux and fixed Q, it is always possible to perform a gauge transformation that moves all information about the topological charge in the system to the border of the lattice, where it will be encoded by transition functions Ω_x, Ω_y such as (3.4). In this case the topological charge can be identified with the number of windings of a scalar field around the border, consistent with the quantisation condition (3.5). It follows that the maximal resolution obtainable is given by the number of points on the perimeter, i.e. the ratio of the length of the perimeter to the step size, since we are not able to probe a field winding a greater number of times than the number of points defining the discrete Fourier transform.

6 Concluding remarks

In this paper we have demonstrated that the spectrum of a simple fermion model formulated on a $2d$ honeycomb lattice does indeed reproduce one of the most important non-

JHEP06(2009)060

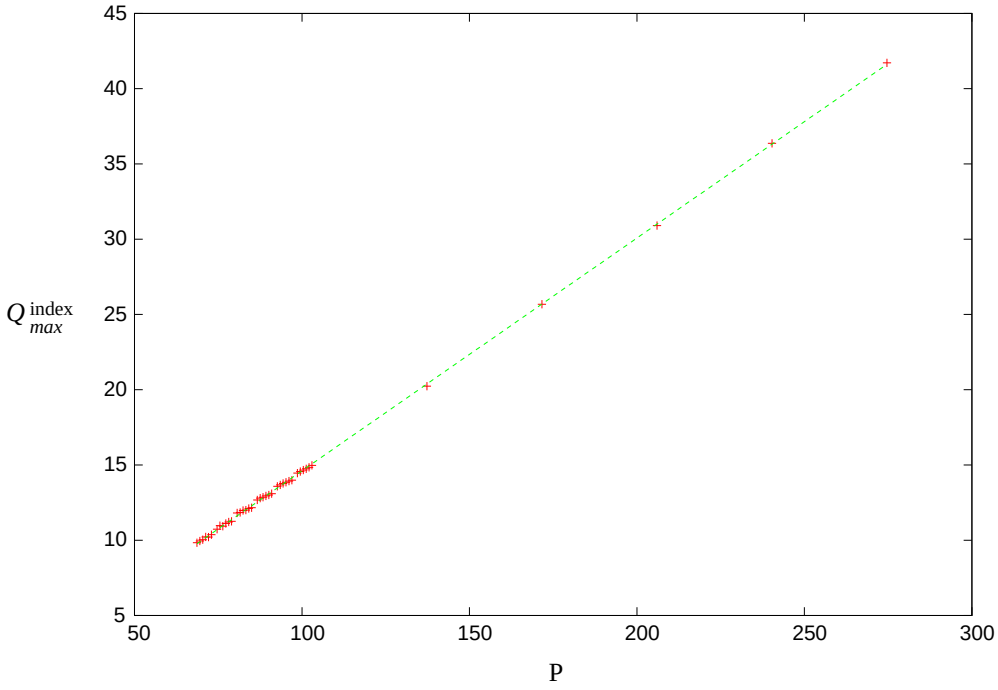

Figure 9. $Q_{\rm max}^{\rm index}$ vs. perimeter P in the perpendicular case

perturbative features of relativistic chiral fermions interacting with a gauge field, namely the index theorem (1.1) relating the number of zero-eigenvalue chiral modes to the background topological charge. We have done this first by calculating the gauge-invariant spectrum in a particularly smooth gauge background and showing that it coincides with analytic expectations yielding zero modes with the correct degeneracy, and next by identifying a suitable chirality operator Σ_3 enabling the index to be calculated. The operator (5.3) distinguishes between fermion fields located on differing A and B sublattices in real space, and between fields localised at differing $\pm$ Dirac points in momentum space. As such it is necessarily not gauge-invariant, and hence has limited practical value except in the artificially-constructed smooth backgrounds used here. Since the spectrum and by extension $\det D$ are gauge-invariant, however, this need not deal a fatal blow to any simulation programme based on honeycomb fermions.

Since we have constructed the operator (5.3) to work on a smooth gauge background, it is legitimate to ask how universal it is, ie. how would it respond in a non-uniform distribution of topological charge, such as that found in the vicinity of a vortex line? In the deep continuum limit all gauge backgrounds can be reduced at least locally to a smooth background by a suitable gauge transformation, where we know (5.3) is appropriate, so it is difficult to see how any alternative definition could be preferred. Nonetheless, it seems likely that $\langle\Sigma_3\rangle$ as defined by (5.3) will be extremely susceptible to lattice artifacts.

We have also studied the maximum $Q_{\rm max}^{\rm index}$ observable in a lattice simulation, and shown that this scales with the lattice perimeter, arguing that the limit is related to the maximum resolution of the discrete Fourier transform along a lattice direction. To our knowledge this is a new observation; it would be interesting to repeat this analysis for staggered lattice

JHEP06(2009)060

fermions on a square lattice.

We close by contrasting what we have found to what is known for staggered lattice fermions. Superficially the two approaches are very similar; one starts with a single-component Grassmann field on each site and then reallocates the degrees of freedom into a new basis to recover fields with spin and flavor quantum numbers appropriate to continuum fermions. The method used by Smit and Vink [8] partitions the original field in momentum space, according to a formalism originally developed in [18]. In that case, however, the 2^d "Dirac points" include the origin, and in contrast to the discussion leading to eq. (2.11), each continuum flavor is evenly distributed across all such points. Bilinears with a specified spin/flavor structure constructed from free fermion fields continue to be applicable in the presence of gauge fields. Moreover a distinct repartition of the fields, based on their relative location in local "hypercubes" each containing 2^d lattice points, is also possible [19], enabling the construction of local gauge-invariant bilinears by suitable insertion of products of link variables. For instance the chirality operator for $2d$ staggered fermions couples χ and $\bar{\chi}$ at opposite corners of an elementary square [8]. The two formalisms coincide in the long-wavelength limit [20]. For honeycomb fermions, the continuum flavors are localised at different Dirac points. We have argued in section 5 that this implies that bilinears appropriate for free fermions need not continue to be correct once gauge interactions are introduced; it is also the case that construction of bilinears such as (5.3) requires a simultaneous reshuffling both in position and in momentum space, making gauge invariance impossible to achieve.

Acknowledgments

The work of DC is supported by the European Commission under project number 39494. We have enjoyed useful discussions with Roberto Auzzi and Agostino Patella.

A Fourier transform on a honeycomb lattice

A.1 Single-valued Fourier transform

The main result we want to obtain in this section is to write down a unique Fourier transform function $\tilde{f}(u, v)$ with a well-defined inverse. Given the peculiar structure of the hexagonal lattice, it will be shown that the range of values of u and v of $\tilde{f}(u, v)$ is larger than for the square case, and depends on the compactification.

To define a Fourier transform we need to expose which elementary translations leave the lattice unchanged; naturally the different types of compactification implement these translations differently. If we want a natural coordinate to enumerate the sites of the lattice we need to define a different support function for each compactification type.

We can then define a support function that defines the location of all the sites of our lattice $\Pi(x, y)$, by dividing the sites into classes, where by a class we mean the subgroup

JHEP06(2009)060

of sites related by a integer combination of elementary translations. It's straightforward to see that for the perpendicular lattice we need four classes to reproduce the entire lattice:

$$\Pi_\perp(x,y) = \sum_{n=0,L_X-1}\sum_{m=0,L_Y/2-1} \delta\Big(x-\frac{3}{2}-3n, y-\sqrt{3}m\Big) + \delta\Big(x-3n, y-\frac{\sqrt{3}}{2}-\sqrt{3}m\Big) + \delta\Big(x-\frac{1}{2}-3n, y-\sqrt{3}m\Big) + \delta\Big(x-2-3n, y-\frac{\sqrt{3}}{2}-\sqrt{3}m\Big), \tag{A.1}$$

while for the primitive lattice we need only two classes:

$$\Pi_p(x,y) = \sum_{n=0,L_0-1}\sum_{n=0,L_1-1} \delta(x-\sqrt{3}n, y-\sqrt{3}m) + \delta\Big(x-\sqrt{3}n-\frac{\sqrt{3}}{2}, y-\sqrt{3}n-\frac{1}{\sqrt{3}}\Big). \tag{A.2}$$

The Fourier transform of any function $f(x,y)$ can then be defined as

$$\tilde{f}(u,v) = \frac{1}{V}\int \mathrm{d}x\mathrm{d}y\ \Pi(x,y)\ f(x,y)\ e^{i\vec{p}\cdot\vec{r}}, \tag{A.3}$$

where $\vec{p}$ is again different for the two compactifications

$$\begin{aligned} \text{Perpendicular} \rightarrow \vec{p} &\equiv \Big(\frac{2\pi}{3L_X}u\ \hat{X}, \frac{4\pi}{\sqrt{3}L_Y}v\ \hat{Y}\Big) \\ \text{Primitive} \rightarrow \vec{p} &\equiv \Big(\frac{2\pi}{\sqrt{3}L_0}u\ \hat{0}, \frac{2\pi}{\sqrt{3}L_1}v\ \hat{1}\Big) \end{aligned} \tag{A.4}$$

This leads to the two different definitions of Fourier transform:

Perpendicular:

$$\begin{aligned} \tilde{f}_\perp(u,v) = \frac{1}{\sqrt{6L_XL_Y}}\sum_{n=0}^{L_X-1}\sum_{m=0}^{L_Y/2-1} e^{-2\pi i\left(\frac{nu}{L_X}+\frac{2mv}{L_Y}\right)}\Bigg[& f_\perp\Big(\frac{3}{2}+3n, \sqrt{3}m\Big)e^{-i\frac{\pi u}{L_X}} \\ & + f_\perp\Big(3n, \frac{\sqrt{3}}{2}+\sqrt{3}m\Big)e^{-i\frac{2\pi v}{L_Y}} + f_\perp\Big(\frac{1}{2}+3n, -\sqrt{3}m\Big)e^{-i\frac{\pi u}{3L_X}} \\ & + f_\perp\Big(2+3n, \frac{\sqrt{3}}{2}+\sqrt{3}m\Big)e^{-i\frac{4\pi u}{3L_X}-i\frac{2\pi v}{L_Y}}\Bigg]. \end{aligned} \tag{A.5}$$

Primitive:

$$\begin{aligned} \tilde{f}_p(u,v) = \frac{1}{3\sqrt{L_0L_1}}\sum_{n=0}^{L_0-1}\sum_{m=0}^{L_1-1} e^{-2\pi i\left(\frac{nu}{L_0}+\frac{mv}{L_1}\right)}\Bigg[& f_p(\sqrt{3}n, \sqrt{3}m) \\ & + f_p\Big(\sqrt{3}n+\frac{2}{\sqrt{3}}, \sqrt{3}m+\frac{1}{\sqrt{3}}\Big)e^{-i2\pi\left(\frac{2u}{3L_0}-\frac{v}{3L_1}\right)}\Bigg]. \end{aligned} \tag{A.6}$$

Now note that the periodicity of the transformed functions so defined differ from the original:

$$\begin{aligned}\tilde{f}_\perp(0,0) &= \tilde{f}_\perp(6L_X, L_Y)\\ \tilde{f}_p(0,0) &= \tilde{f}_p(3L_0, 3L_1).\end{aligned} \tag{A.7}$$

To define the inverse transform we cannot define an unique formula for all classes. Rather, the inverse must be calculated on each class separately.

Perpendicular:

$$\begin{aligned}
f_\perp\left(\frac{3}{2}+3n, \sqrt{3}m\right) &= \frac{1}{\sqrt{6L_XL_Y}}\sum_{u=0}^{6L_X-1}\sum_{v=0}^{L_Y-1} e^{2\pi i\left(\frac{nu}{L_X}+\frac{2mv}{L_Y}\right)}\tilde{f}_\perp(u,v)e^{i\frac{\pi u}{L_X}}\\
f_\perp\left(3n, \frac{\sqrt{3}}{2}+\sqrt{3}m\right) &= \frac{1}{\sqrt{6L_XL_Y}}\sum_{u=0}^{6L_X-1}\sum_{v=0}^{L_Y-1} e^{2\pi i\left(\frac{nu}{L_X}+\frac{2mv}{L_Y}\right)}\tilde{f}_\perp(u,v)e^{i\frac{2\pi v}{L_Y}}\\
f_\perp\left(\frac{1}{2}+3n, -\sqrt{3}m\right) &= \frac{1}{\sqrt{6L_XL_Y}}\sum_{u=0}^{6L_X-1}\sum_{v=0}^{L_Y-1} e^{2\pi i\left(\frac{nu}{L_X}+\frac{2mv}{L_Y}\right)}\tilde{f}_\perp(u,v)e^{i\frac{\pi u}{3L_X}}\\
f_\perp\left(2+3n, \frac{\sqrt{3}}{2}+\sqrt{3}m\right) &= \frac{1}{\sqrt{6L_XL_Y}}\sum_{u=0}^{6L_X-1}\sum_{v=0}^{L_Y-1} e^{2\pi i\left(\frac{nu}{L_X}+\frac{2mv}{L_Y}\right)}\tilde{f}_\perp(u,v)e^{i\frac{4\pi u}{3L_X}+i\frac{2\pi v}{L_Y}}
\end{aligned} \tag{A.8}$$

Primitive:

$$f_p(\sqrt{3}n, \sqrt{3}m) = \frac{1}{3\sqrt{L_0L_1}}\sum_{u=0}^{3L_0-1}\sum_{v=0}^{3L_1-1} e^{2\pi i\left(\frac{nu}{L_0}+\frac{mv}{L_1}\right)}\tilde{f}_p(u,v) \tag{A.9}$$

$$f_p\left(\sqrt{3}n+\frac{2}{\sqrt{3}}, \sqrt{3}m+\frac{1}{\sqrt{3}}\right) = \frac{1}{3\sqrt{L_0L_1}}\sum_{u=0}^{3L_0-1}\sum_{v=0}^{3L_1-1} e^{2\pi i\left(\frac{nu}{L_0}+\frac{mv}{L_1}\right)}\tilde{f}_p(u,v)e^{2\pi i\left(\frac{2u}{3L_0}+\frac{v}{3L_1}\right)}$$

A.2 Multi-valued Fourier transform

If we relax the requirement of having a single-valued function of momentum, but still wish to expose the different structure of the A and B sites in the Fourier transform, we obtain two further definitions. In this case the the range of values of u and v depends on the compactification, but is always smaller than the previous case. The procedure to obtain these function is totally equivalent to the previous case, so here we only show the results.

Perpendicular:

$$\tilde{f}_{\perp}^{(A)}(u,v) = \frac{1}{\sqrt{2L_XL_Y}} \sum_{n=0}^{L_X-1} \sum_{m=0}^{L_Y/2-1} e^{-2\pi i\left(\frac{nu}{L_X}+\frac{2mv}{L_Y}\right)} \left[f_{\perp}\left(\frac{3}{2}+3n, \sqrt{3}m\right) e^{-i\frac{\pi u}{L_X}} + f_{\perp}\left(3n, \frac{\sqrt{3}}{2}+\sqrt{3}m\right) e^{-i\frac{2\pi v}{L_Y}} \right]$$

$$\tilde{f}_{\perp}^{(B)}(u,v) = \frac{1}{\sqrt{2L_XL_Y}} \sum_{n=0}^{L_X-1} \sum_{m=0}^{L_Y/2-1} e^{-2\pi i\left(\frac{nu}{L_X}+\frac{2mv}{L_Y}\right)} \left[f_{\perp}\left(\frac{1}{2}+3n, -\sqrt{3}m\right) e^{-i\frac{\pi u}{3L_X}} + f_{\perp}\left(2+3n, \frac{\sqrt{3}}{2}+\sqrt{3}m\right) e^{-i\frac{4\pi u}{3L_X}-i\frac{2\pi v}{L_Y}} \right]. \quad \text{(A.10)}$$

Perpendicular Inverse:

$$\begin{aligned}
f_{\perp}\left(\frac{3}{2}+3n, \sqrt{3}m\right) &= \frac{1}{\sqrt{2L_XL_Y}} \sum_{u=0}^{2L_X-1} \sum_{v=0}^{L_Y-1} e^{2\pi i\left(\frac{nu}{L_X}+\frac{2mv}{L_Y}\right)} \tilde{f}_{\perp}^{(A)}(u,v) e^{i\frac{\pi u}{L_X}} \\
f_{\perp}\left(3n, \frac{\sqrt{3}}{2}+\sqrt{3}m\right) &= \frac{1}{\sqrt{2L_XL_Y}} \sum_{u=0}^{2L_X-1} \sum_{v=0}^{L_Y-1} e^{2\pi i\left(\frac{nu}{L_X}+\frac{2mv}{L_Y}\right)} \tilde{f}_{\perp}^{(A)}(u,v) e^{i\frac{2\pi v}{L_Y}} \\
f_{\perp}\left(\frac{1}{2}+3n, -\sqrt{3}m\right) &= \frac{1}{\sqrt{2L_XL_Y}} \sum_{u=0}^{2L_X-1} \sum_{v=0}^{L_Y-1} e^{2\pi i\left(\frac{nu}{L_X}+\frac{2mv}{L_Y}\right)} \tilde{f}_{\perp}^{(B)}(u,v) e^{i\frac{\pi u}{3L_X}} \\
f_{\perp}\left(2+3n, \frac{\sqrt{3}}{2}+\sqrt{3}m\right) &= \frac{1}{\sqrt{2L_XL_Y}} \sum_{u=0}^{2L_X-1} \sum_{v=0}^{L_Y-1} e^{2\pi i\left(\frac{nu}{L_X}+\frac{2mv}{L_Y}\right)} \tilde{f}_{\perp}^{(B)}(u,v) e^{i\frac{4\pi u}{3L_X}+i\frac{2\pi v}{L_Y}}
\end{aligned} \quad \text{(A.11)}$$

Primitive:

$$\begin{aligned}
\tilde{f}_{p}^{(A)}(u,v) &= \frac{1}{\sqrt{L_0L_1}} \sum_{n=0}^{L_0-1} \sum_{m=0}^{L_1-1} e^{-2\pi i\left(\frac{nu}{L_0}+\frac{mv}{L_1}\right)} f_p(\sqrt{3}n, \sqrt{3}m) \\
\tilde{f}_{p}^{(B)}(u,v) &= \frac{1}{\sqrt{L_0L_1}} \sum_{n=0}^{L_0-1} \sum_{m=0}^{L_1-1} e^{-2\pi i\left(\frac{nu}{L_0}+\frac{mv}{L_1}\right)} f_p\left(\sqrt{3}n+\frac{2}{\sqrt{3}}, \sqrt{3}m+\frac{1}{\sqrt{3}}\right) e^{-i2\pi\left(\frac{2u}{3L_0}-\frac{v}{3L_1}\right)}
\end{aligned} \quad \text{(A.12)}$$

Primitive Inverse:

$$\begin{aligned}
f_p(\sqrt{3}n, \sqrt{3}m) &= \frac{1}{\sqrt{L_0L_1}} \sum_{u=0}^{L_0-1} \sum_{v=0}^{L_1-1} e^{2\pi i\left(\frac{nu}{L_0}+\frac{mv}{L_1}\right)} \tilde{f}_{p}^{(A)}(u,v) \\
f_p\left(\sqrt{3}n+\frac{2}{\sqrt{3}}, \sqrt{3}m+\frac{1}{\sqrt{3}}\right) &= \frac{1}{\sqrt{L_0L_1}} \sum_{u=0}^{L_0-1} \sum_{v=0}^{L_1-1} e^{2\pi i\left(\frac{nu}{L_0}+\frac{mv}{L_1}\right)} \tilde{f}_{p}^{(B)}(u,v) e^{2\pi i\left(\frac{2u}{3L_0}+\frac{v}{3L_1}\right)}
\end{aligned}$$

JHEP06(2009)060

References

[1] L.H. Karsten, *Lattice fermions in euclidean space-time*, *Phys. Lett.* **B 104** (1981) 315 [SPIRES];
F. Wilczek, *On lattice fermions*, *Phys. Rev. Lett.* **59** (1987) 2397 [SPIRES].

[2] M. Creutz, *Four-dimensional graphene and chiral fermions*, *JHEP* **04** (2008) 017 [arXiv:0712.1201] [SPIRES].

[3] A. Boriçi, *Creutz fermions on an orthogonal lattice*, *Phys. Rev.* **D 78** (2008) 074504 [arXiv:0712.4401] [SPIRES].

[4] P.F. Bedaque, M.I. Buchoff, B.C. Tiburzi and A. Walker-Loud, *Broken symmetries from minimally doubled fermions*, *Phys. Lett.* **B 662** (2008) 449 [arXiv:0801.3361] [SPIRES].

[5] K. Cichy, J. Gonzalez Lopez, K. Jansen, A. Kujawa and A. Shindler, *Twisted mass, overlap and Creutz fermions: cut-off effects at tree-level of perturbation theory*, *Nucl. Phys.* **B 800** (2008) 94 [arXiv:0802.3637] [SPIRES].

[6] H.B. Nielsen and M. Ninomiya, *Absence of neutrinos on a lattice. 1. Proof by homotopy theory*, *Nucl. Phys.* **B 185** (1981) 20 [*Erratum ibid.* **B 195** (1982) 541] [SPIRES]; *Absence of neutrinos on a lattice. 2. Intuitive topological proof*, *Nucl. Phys.* **B 193** (1981) 173 [SPIRES].

[7] M. Creutz, *Local chiral fermions*, arXiv:0808.0014 [SPIRES].

[8] J. Smit and J.C. Vink, *Remnants of the index theorem on the lattice*, *Nucl. Phys.* **B 286** (1987) 485 [SPIRES].

[9] P.F. Bedaque, M.I. Buchoff, B.C. Tiburzi and A. Walker-Loud, *Search for fermion actions on hyperdiamond lattices*, *Phys. Rev.* **D 78** (2008) 017502 [arXiv:0804.1145] [SPIRES].

[10] G.W. Semenoff, *Condensed matter simulation of a three-dimensional anomaly*, *Phys. Rev. Lett.* **53** (1984) 2449 [SPIRES].

[11] R. Jackiw, *Fractional charge and zero modes for planar systems in a magnetic field*, *Phys. Rev.* **D 29** (1984) 2375 [*Erratum ibid.* **D 33** (1986) 2500] [SPIRES].

[12] V.P. Gusynin and S.G. Sharapov, *Unconventional integer quantum Hall effect in graphene*, *Phys. Rev. Lett.* **95** (2005) 146801 [cond-mat/0506575] [SPIRES];
Y. Hatsugai, T. Fukui and H. Suzuki, *Topological analysis of the quantum Hall effect in graphene: Dirac-Fermi transition across van Hove singularities and edge versus bulk quantum numbers*, *Phys. Rev.* **B 74** (2006) 205414.

[13] J.K. Pachos and M. Stone, *An index theorem for graphene*, *Int. J. Mod. Phys.* **B 21** (2007) 5113 [cond-mat/0607394] [SPIRES].

[14] R. Jackiw and S.Y. Pi, *Chiral gauge theory for graphene*, cond-mat/0701760 [SPIRES].

[15] Y. Saad, *Numerical methods for large eigenvalue problems*, Manchester University Press, Manchester U.K. (1992).

[16] L. Del Debbio, L. Giusti, M. Lüscher, R. Petronzio and N. Tantalo, *Stability of lattice QCD simulations and the thermodynamic limit*, *JHEP* **02** (2006) 011 [hep-lat/0512021] [SPIRES].

[17] U.R. Alim and T. Möller, *A discrete Fourier transform for the hexagonal and body-centered lattices*, SFU Computing Science Technical Report 2008-14;

JHEP06(2009)060

A. Vince and X. Zheng, *Computing the discrete Fourier transform on a hexagonal lattice*, *J. Math. Imaging Vis.* **28** (2007) 125.

[18] C. van den Doel and J. Smit, *Dynamical symmetry breaking in two flavor* SU(N) *and* SO(N) *lattice gauge theories*, *Nucl. Phys.* **B 228** (1983) 122 [SPIRES].

[19] H. Kluberg-Stern, A. Morel, O. Napoly and B. Petersson, *Flavors of lagrangian Susskind fermions*, *Nucl. Phys.* **B 220** (1983) 447 [SPIRES].

[20] D. Daniel and T.D. Kieu, *On the flavor interpretations of staggered fermions*, *Phys. Lett.* **B 175** (1986) 73 [SPIRES].

JHEP06(2009)060